Commun Nonlinear Sci Numer Simulat 67 (2019) 568–576

Contents lists available at ScienceDirect

Commun Nonlinear Sci Numer Simulat

journal homepage: www.elsevier.com/locate/cnsns

Research paper

Extended self-similarity based multi-fractal detrended fluctuation analysis: A novel multi-fractal quantifying method

Da Nian, Zuntao Fu*

Lab for Climate and Ocean-Atmosphere Studies, Department of Atmospheric and Oceanic Sciences, School of Physics, Peking University, Beijing 100871, China

ARTICLE INFO

Article history:
Received 11 May 2018
Revised 9 July 2018
Accepted 24 July 2018
Available online 26 July 2018

Keywords:
MF-DFA
ESS
ESS-MF-DFA
Scaling range
Multi-fractal strength

ABSTRACT

Based on multi-fractal detrended fluctuation analysis (MF-DFA) method, the extended self-similarity (ESS) is incorporated to develop a novel method to quantify multi-fractal characteristics. Detailed results show that compared with MF-DFA this new extended self-similarity based MF-DFA (ESS-MF-DFA) method can significantly extend scaling range and reduce uncertainties in estimating the exponents. Moreover, although ESS-MF-DFA method is developed from the DFA method with a fundamental assumption of a definite scaling range between fluctuation function and scale, ESS-MF-DFA can still work well even when DFA fails due to no scaling range between fluctuation function and scale. Furthermore, a criterion without estimating the generalized Hurst exponents is developed based on ESS-MF-DFA to distinguish multi-fractal from mono-fractal behavior and to quantify multi-fractal strength. All these results indicate that ESS-MF-DFA outperforms MF-DFA in reliably handling multi-fractal quantifications for much wider fields.

1. Introduction

Long-term persistence (or fractal behavior) is ubiquitous in real world, and is a significant feature in time series analysis. The time series from complex system exhibiting long-term persistence in nature, e.g. DNA sequences, can be characterized by a power law relation [1–3]. They may exhibit mono-fractal scaling behavior in spectral analysis with a single scaling exponent, which is the simplest case. Or, they may exhibit multi-fractal scaling behavior with different scaling exponents to depict the different scaling behaviors from variation of fluctuations [4]. This complicated character results in the well establishment of multi-fractal theory, which has already been utilized in many fields, such as climatology, turbulence, finance, ecology, physiology, geophysics and many other fields. Multi-fractal theory makes profound impacts on studying nonlinear features and complex dynamical details in various physical phenomena [5], and plays a fundamental role in signals identification and trend prediction [6–8]. In the progress of deeper understanding multi-fractal theory, what has caught our attention is that it is becoming much urgent to accurately differentiate multi-fractal from mono-fractal characteristic through reasonable quantitative criteria.

Since the critical achievement of detrended fluctuation analysis (DFA) method by Peng et al. [2], which could detect long-term persistence or (mono-) fractal scaling properties in time series, multi-fractal detrended fluctuation analysis (MF-DFA) method [4] is developed to identify multi-fractal behaviors based on DFA method.

* Corresponding author.
E-mail address: fuzt@pku.edu.cn (Z. Fu).

https://doi.org/10.1016/j.cnsns.2018.07.034
1007-5704/

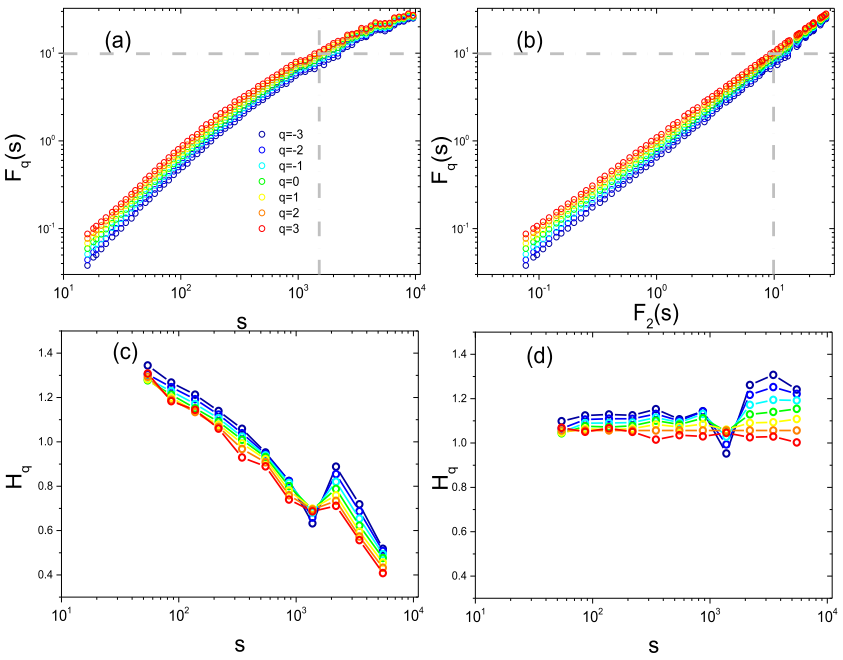

Fig. 1. Scaling range of boundary layer wind speed defined in (a) MF-DFA. (b) ESS-MF-DFA. The gray dash lines denote the same position in (a) and (b). The variation of local Hurst exponent with scale derived from (c) MF-DFA. (d) ESS-MF-DFA. The different colors from blue to red correspond to $H(q)$ of q from −3 to 3. (For interpretation of the references to colour in this figure legend, the reader is referred to the web version of this article.)

MF-DFA method is widely adopted to quantify multi-fractal properties in recent years [5–9]. For the time series with long-term persistence, there exists $F_q(s) \sim s^{H(q)}$, where $H(q)$ is the generalized Hurst exponent, $F_q(s)$ is qth-order fluctuation function, and s is the scale. For multi-fractal time series, $H(q)$ is significantly dependent on q, and $H(q)$ varies with q (Details of MF-DFA method can be seen at Methods section). If q is positive, $H(q)$ describes the scaling behavior of large fluctuations, while $H(q)$ with negative q describes the scaling behavior of small fluctuations. For mono-fractal time series, $H(q)$ is independent of q [4]. Usually, proceeding a log computation obtains

$$\log_{10} F_q(s) \sim H(q) \log_{10} s. \tag{1}$$

Then we can get $H(q)$ through linear fitting directly within a scaling range, and $\Delta H_q = \max H_q - \min H_q$ could give a simple quantification for multi- or mono- fractal strength with a finite range of q. In this article, we choose q ranging from −3 to 3, which ensures the ability to distinguish multi-fractal from mono-fractal behavior with limited data size [10].

However, limitations are clear for both DFA and MF-DFA method. Both of them require a definite scaling range to estimate the related scaling exponents. This scaling range, or called fitting region, is difficult to determine, because the scaling exponent is very sensitive to the selected range [9]. Subtle changes of the selected scaling range can cause a dramatic variation on estimation of scaling exponent. More importantly, there is no objective criterion for the determination of scaling range in many studies [2,11]. Previous research has provided a criterion based on crossover time scales for the determination of optimal scaling ranges in DFA and MF-DFA [9]. However, this kind of criterion does not work well in all circumstances. For example, it fails for the case that the selected scaling range is very narrow, or even too narrower to define, just the case for wind records (Fig. 1a). So segmented fitting has been performed to the fluctuation function over large and small scales, respectively [12]. Moreover, the scaling exponent also could be estimated through fitting the fluctuation function directly [5]. Both of these cases may not be convincing. Thus, consistent results for quantifying the multi-fractal strength of time series could not be fulfilled using DFA and MF-DFA method. Accurate estimation of the multi-fractal strength is far more important for this circumstance.

So the first problem in DFA or MF-DFA related studies is how to extend the scaling ranges if they do exist. Secondly, how to reduce the uncertainties of the estimated scaling exponents when a definite scaling range does exist? What's more, if there is no scaling range in DFA or MF-DFA results, can MF-DFA still be employed with certain modification to quantify the multi-fractal strength? Can this modification provide a reasonable quantification to differentiate the multi-fractal from mono-fractal feature? Extended self-similarity (ESS) found in fluid turbulence may provide us the right solution in dealing with the problems above, since a scaling range can be extended strikingly wider [13]. Inspired by ESS, we can solve problems by creatively incorporating the ESS to MF-DFA to develop a novel method, extended self-similarity based MF-DFA (ESS-MF-DFA). Further details of ESS-MF-DFA method will be shown in the Method section.

In this paper, contrast with the results of MF-DFA, we will show how ESS-MF-DFA can improve the quantification of multi-fractal strength. The advantages of ESS-MF-DFA to deal with the above problems will be introduced by conducting

two numerical tests. Further, the utility of ESS-MF-DFA is confirmed by the observed boundary-layer wind speed data. The first test is an idealized long-range correlated mono-fractal series, where the generalized Hurst exponent $H(q)$ is supposed to be independent of q. Fourier transform method [14] is employed to generate 100 repeated simulated long-range correlated time series with a given Hurst exponent H. The results from both MF-DFA and ESS-MF-DFA show the ability of ESS-MF-DFA to extend the scaling range and to reduce the uncertainties in estimating the scaling exponents compared with MF-DFA. The second test is multi-fractal series generated from binomial multi-fractal model [4,14], where the generalized Hurst exponent $H(q)$ is known for given a and q. The generalized scaling exponent function $H(q)$ has an analytic form [14],

$$H(q) = \frac{1}{q} - \frac{\ln\left[a^q + (1-a)^q\right]}{q\ln(2)}. \tag{2}$$

Since each $H(q)$ is exactly known from Eq. (2) for each generated series, we can clearly get the idea how well the ESS-MF-DFA estimates each $H(q)$ with much smaller uncertainties over wider scaling range and extract the multi-fractal strength compared with MF-DFA. In the end, the observed wind speed within atmospheric boundary layer has been analyzed. It is shown that ESS-MF-DFA can truly accurately quantify multi-fractal features in the real case where no scaling range exists in DFA.

2. Data and methods

2.1. Data

2.1.1. Measured data

Observed boundary-layer wind speed data used here are provided by the field experiment in Huaihe River Basin from 9 to 22 June 1998. The observation field is located at the western edge of a large paddy field. The wind velocity component has been measured through a three-dimensional sonic anemometer (SAT-211/3 K, sampling rate 10 Hz, located 4 m above ground). The more details can be found in the Ref. [15–20]. This data set has been widely used to analyze nonlinear features and properties of turbulence in the atmospheric boundary layer [18–20]. We analyzed 12 time series of the measured data, and obtained the same result as showed in Fig. 1.

2.1.2. Description and preprocessing of the data

For mono-fractal model, 100 time series of length 20,000 with a given Hurst exponent were generated. When Hurst exponent below 0.5, we first estimate the scaling exponent α' of the integrated data and then obtain α by $\alpha = \alpha' - 1$ [21,22].

For binomial multi-fractal model, the time series satisfy $x_k = a^{n(k-1)}(1-a)^{n_{max}-n(k-1)}$, where the length $N = 2^{n_{max}}$ and $k = 1, \ldots, N$ with parameter $0.5 < a < 1$. And $n(k)$ is the number of digits 1 in the binary form of the index k. Here, the 100 time series of length 20,000 for given a were generated. And the cases for $q = -3, -2, -1, 0, 1, 2, 3$ were analyzed in this paper.

The exponents of the fluctuation function $F_q(s)$ are estimated at 73 s-values logarithmically sampled in the interval [4,4570] for both methods. For each time series, we calculated the local slope of $\log_{10}F_q(s)$ fitting in the moving window. The length of every moving window is 10 s-values logarithmically, and every 5 s-values logarithmically move a step forward.

2.2. Methods

2.2.1. MF-DFA method

In this subsection, we briefly explain the algorithm of the MF-DFA method [4], more detailed steps can be found in the Ref. [4].

Consider a time series $\{x(t),\ t = 1, 2, \ldots, N\}$ with zero mean, the profile $y(t)$ can be calculated by the cumulative sum of $x(t)$. Divide $y(t)$ into N_s nonoverlapping segments of equal length s. And similar calculating can be repeated starting from the opposite end. Thereby, $2N_s$ segments are gotten. Calculate the local trend of each segment, and the variance is

$$F^2(v,s) = \frac{1}{s}\sum_{i=1}^{s}\{y[(v-1)s+i] - t_v(i)\}^2, \tag{3}$$

where $t_v(i)$ is the fitting polynomial in segment v. There are linear, quadratic or high order polynomials available to fit which corresponds to MF-DFA1, MF-DFA2, etc. [4]. In this article, we choose MF-DFA3 for comparison. Average over all segments to lead to the qth order fluctuation function:

$$F_q(s) \equiv \left\{\frac{1}{2N_s}\sum_{v=1}^{2N_s}\left[F^2(v,s)^{q/2}\right]^{1/q}\right\}, \tag{4}$$

where q can take any real value [4]. For $q = 2$, Eq .(4) is the standard DFA procedure.

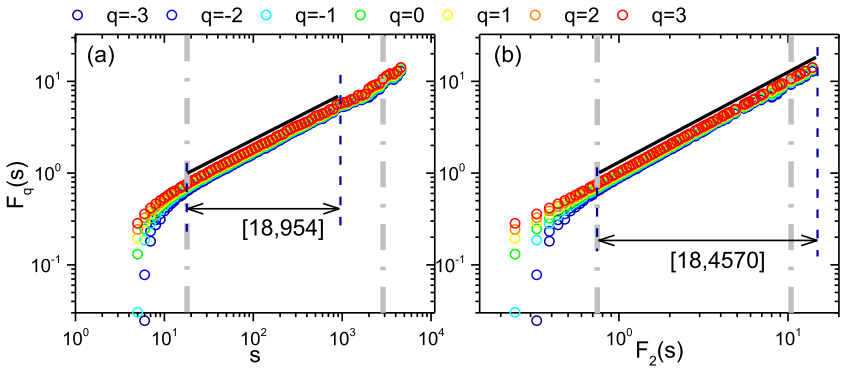

Fig. 2. Scaling range (within two dark dash vertical lines) of a realization of mono-fractal series with $H = 0.5$. (a) [18,954] by MF-DFA . (b) [18,4570] by ESS-MF-DFA. The length of time series is 20,000 and the different colors for the different values of the exponent q from −3 to 3. The grey dash lines indicate the same position in different coordinates.

It is worth noting that when $q = 0$, Eq .(4) can't be used to determine $H(0)$ directely. Instead, one can adopt a logarithmic average procedure [4],

$$F_0(s) = \exp\left\{\frac{1}{4N_s}\sum_{v=1}^{2N_s}\ln\left[F^2(v,s)\right]\right\} \sim s^{H(0)}, \tag{5}$$

In this paper, we set $q = -3, -2, -1, 0, 1, 2, 3$.

2.2.2. ESS-MF-DFA method

Benzi et al. discovered ESS in studies of the velocity differences of turbulent flows [13]. The structure function (SF) of the velocity increments $\Delta V(r)$ of turbulent flows exhibits a well-defined scaling law:

$$\left\langle \Delta V(r)^3 \right\rangle \approx r^{\xi(3)}\ , \left\langle \left|\Delta V(r)^n\right| \right\rangle = B_n \left\langle \left|\Delta V(r)^3\right| \right\rangle^{\xi(n)}. \tag{6}$$

They found that there are considerable statistical errors due to the limited scaling range in the log-log relations of $\langle \Delta V(r)^2 \rangle$ vs r and $\langle \Delta V(r)^3 \rangle$ vs r. This case is similar to what we encountered with the scaling behaviors of fluctuation functions under DFA or MF-DFA method. Then they discovered an impressive wider scaling range for $\langle \Delta V(r)^2 \rangle$ versus $\langle \Delta V(r)^3 \rangle$. Similar results [13] with much wider scaling range hold for $\langle |\Delta V(r)^n| \rangle$ versus $\langle \Delta V(r)^3 \rangle$ with $n > 3$.

When calculating the qth order fluctuation function $F_q(s)$ for a time series, from Eq. (1), one can obtain

$$\log_{10}(F_q(s)) \sim A_{q,q'}\log_{10}(F_{q'}(s)),\ A_{q,q'} = \frac{H(q)}{H(q')} \tag{7}$$

where q and q' can be different, and $H(q') \neq 0$. It can be found that Eq. (7) is similar to Eq. (6) and it defines a novel method to modify the MF-DFA. Given by ESS consideration, we use $A_{q,q'}$ instead of $H(q)$ to quantify multi-fractal properties.

$\Delta H_q = \max H_q - \min H_q$ has been applied to quantify the multi-fractal strength in MF-DFA [10]. Similarly, we get

$$\Delta A_q = \max A_q - \min A_q. \tag{8}$$

Where $\Delta H_q = \Delta A_q * H(q')$, and $H(q')$ is a constant. In this paper, we let $q' = 2$, and $H(q') = H(2)$ that can be estimated by DFA procedure. Since there are much wider scaling range and smaller uncertainties in ESS-MF-DFA (see the results section), and this indicates that there are ***much smaller uncertainties*** in determining ΔA_q than in ΔH_q.

What's more, ΔA_q is ***completely independent*** of the value of $H(q')$. Thereby, The error and uncertainty caused by the estimation of $H(q')$ are completely independent of ΔA_q. So ΔA_q can be taken as a better measure to distinguish multi-fractal from mono-fractal series compared with ΔH_q, and ESS-MF-DFA method may accurately capture multi-fractal information. Detailed results will be shown in the next section.

3. Results

3.1. Wider scaling range of ESS-MF-DFA compared with MF-DFA

Firstly, the test based on mono-fractal model reveals the ability for ESS-MF-DFA to enlarge the estimated scaling range. Fig. 2 demonstrates the results. When the scale s is large, the straightness of fluctuation functions changing with scale for all $q \in [-3, 3]$ in ESS-MF-DFA is remarkable, while the fluctuation functions changing with scale depart larger in MF-DFA. The scaling range is much wider in ESS-MF-DFA ([18,4570], see Fig. 2(b)) than in MF-DFA ([18,954], see Fig. 2(a)). Furthermore, the wider scaling range in ESS-MF-DFA can be seen vividly in local Hurst exponents compared with the narrower scaling

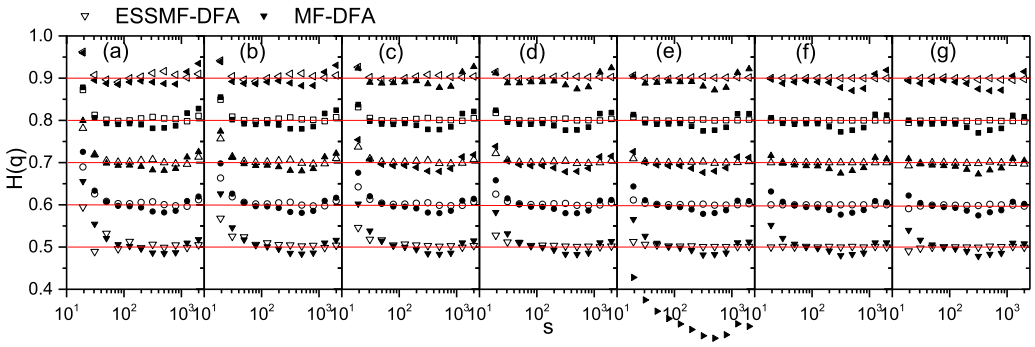

Fig. 3. Averaged local Hurst exponents obtained by MF-DFA (solid) and ESS-MF-DFA (open) over 100 repeated simulations with 5 fixed Hurst exponents ($H = 0.5,\ 0.6,\ 0.7,\ 0.8,\ 0.9$). Each column corresponds to results for a fixed q ($q = -3,\ -2,\ -1,\ 0,\ 1,\ 2,\ 3$, from left to right). The red solid line indicates the theoretical Hurst exponent. (For interpretation of the references to colour in this figure legend, the reader is referred to the web version of this article.)

Table 1
$\overline{H(q)}$, $\sigma_{H(q)}$ and linear fit of goodness parameters (SSE and R-square) within scaling range by MF-DFA and ESS-MF-DFA over 100 repeated simulations for mono-fractal model with $H = 0.7$.

q		−3	−2	−1	1	2	3	−3
$\overline{H(q)}$	MF-DFA	0.6959	0.6947	0.6938	0.6931	0.6923	0.6912	0.6898
	ESS-MF-DFA	0.7044	0.7033	0.7024	0.7017	0.7010	0.7000	0.6986
$\sigma_{H(q)}$	MF-DFA	0.0239	0.0239	0.0242	0.0249	0.0260	0.0274	0.0288
	ESS-MF-DFA	0.0140	0.0117	0.0090	0.0061	0.0031	0.0000	0.0029
SSE	MF-DFA	0.0173	0.0155	0.0145	0.0144	0.0153	0.0173	0.0203
	ESS-MF-DFA	0.0119	0.0082	0.0050	0.0024	0.0006	0.0000	0.0006
R-square	MF-DFA	0.9976	0.9978	0.9980	0.9980	0.9979	0.9976	0.9972
	ESS-MF-DFA	0.9983	0.9989	0.9993	0.9997	0.9999	1.0000	0.9999

range in MF-DFA, see Fig. 3. The mean local Hurst exponents from 100 simulations of mono-fractal models indicate that there are much wider plateaus closed to the theoretical exponents in ESS-MF-DFA, while there are no or much narrower plateaus closed to the theoretical exponents in MF-DFA.

In the following, we will further illustrate the ability of ESS-MF-DFA in enlarging the scaling range by revisiting the observed wind speed data, which has no definite scaling based on MF-DFA method, see Fig. 1(a). When scale s is larger than 300 in Fig. 1(a), power law assumption in MF-DFA is not valid for each q (scaling range is too narrower to define). Thus right now MF-DFA lost the ability to estimate each $H(q)$ in boundary-layer wind speed at the larger scales. However, ESS-MF-DFA is capable of estimating it. When using the ESS-MF-DFA, in Eq. (7), let $q' = 2$ (the 2th order fluctuation function $F_2(s)$ as the abscissa) and the ordinate is qth order fluctuation function $F_q(s)$. Then a definite wider scaling range can be found, see Fig. 1(b), where the scaling range in MF-DFA below $s = 300$ is extended to the whole range in ESS-MF-DFA. The slopes $A_q = A_{q,2}$ for each qth $F_q(s)$ versus $F_2(s)$ in log-log plot can be obtained through linear fitting. In order to compare with results based on MF-DFA method, the estimated slope needs to be converted to generalized Hurst exponent $H(q)$. According to Eq. (7), there exists $H(q) = A_q \times H(2)$, then we reach $H(q)$ through ESS-MF-DFA procedure.

As we can see, ESS-MF-DFA method effectively solves the problem where the scaling range is too narrower to define in MF-DFA for some cases just like boundary-layer wind speed. Fig. 1(c) and (d) compare the scaling range of results calculated with two methods (MF-DFA and ESS-MF-DFA). It is noticed that the MF-DFA results of boundary layer wind speed confirm those results in the Ref. [5,12], which demonstrates local Hurst exponents from MF-DFA changing dramatically with scale (Fig. 1(c)). There are no plateaus in local Hurst exponents from MF-DFA to define a definite scaling range. When ESS-MF-DFA method is considered, there are marked plateaus in local Hurst exponents (Fig. 1(d)) with a much wider scaling range. Although ESS-MF-DFA is derived from DFA based on the power law relationship between fluctuation function and scale, it works well even DFA fails to work, i.e., there is no definite scaling between fluctuation function and scale (***power law assumption is not valid***).

3.2. Smaller uncertainties in ESS-MF-DFA than in MF-DFA

In order to perform the multi-fractal analysis over the variables in real world using MF-DFA or ESS-MF-DFA method, it is of vital necessity to improve accuracy of estimated exponents for each q. In fact, wider scaling range will reduce the error in estimating exponents for each q, and then ESS-MF-DFA method can work better than MF-DFA in improving accuracy of estimated exponents for each q, see Fig. 4. For both methods, standard errors are small at small scales while large at large scales. ESS-MF-DFA method performs better than MF-DFA at all scales, especially when q is positive. In detail, 100 repeated simulations for a mono-fractal model with $H = 0.7$ are shown in Table 1, where the fitting parameters (mean

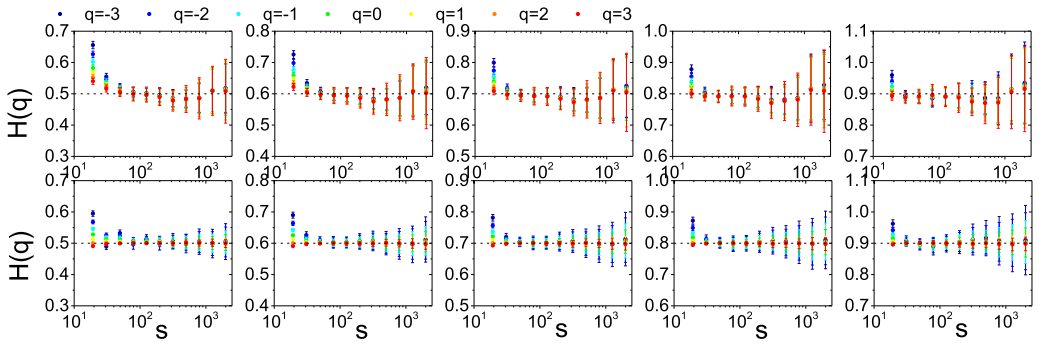

Fig. 4. Uncertainties of estimated $\overline{H(q)}$ quantified by $\sigma_{H(q)}$ over 100 repeated simulations. Each plot includes results from seven fixed q ($q = -3,\ -2,\ -1,\ 0,\ 1,\ 2,\ 3$) obtained by MF-DFA (top row) and ESS-MF-DFA (bottom row). Each column corresponds to results for a Hurst exponent ($H = 0.5,\ 0.6,\ 0.7,\ 0.8,\ 0.9$, from left to right). The black dash line corresponds the theoretical Hurst exponent.

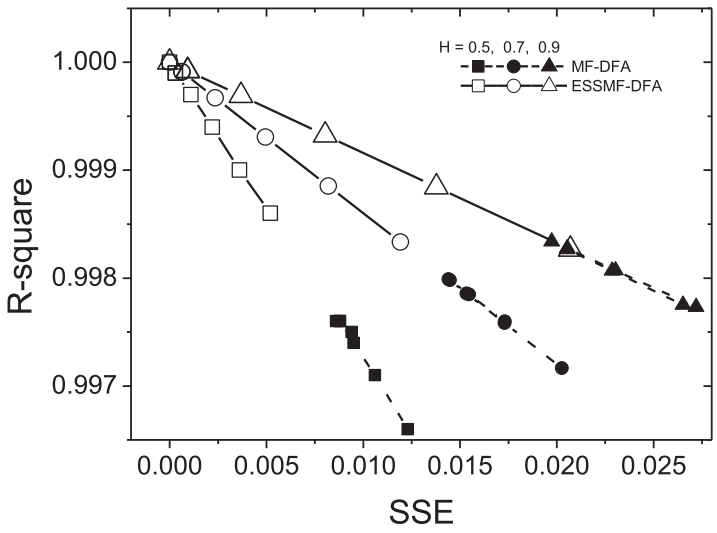

Fig. 5. Scatter plot of R-square vs. SSE for three Hurst exponents: $H = 0.5$(■, □), $H = 0.7$(●, ○), $H = 0.9$(▲, △). Solid symbol stands for results from MF-DFA, and open symbol stands for results from ESS-MF-DFA.

Hurst exponents and their standard deviations, R squares and fitted sum of squared error (SSE) for linear fit of goodness) have been calculated over the same scaling range. It is obvious that ESS-MF-DFA method extremely reduces SSE and standard deviation with increasing R square simultaneously. SSE stands for the difference between true and fitting results, and the smaller the SSE, the closer to the true value. The results shown in Fig. 4 and Table 1 indicate that the results of ESS-MF-DFA are closer to the true value. And ESS-MF-DFA performs better than MF-DFA for all $q \in [-3, 3]$, and this can be seen much clearer in the scatter plot of R square vs. SSE in Fig. 5. The best fitting with smaller uncertainties in estimating the exponents for each q is that R square is close to 1 and SSE is close to zero simultaneously, i.e., in the up-left corner on the scatter plot of R square vs. SSE (corresponding to ESS-MF-DFA results). On the contrary, larger uncertainties have been found in the down-right corner of the scatter plot of R square vs. SSE (corresponding to MF-DFA results). So ESS-MF-DFA method can improve accuracy of the estimated exponents for each q, which makes the overall fitting enhanced compared with MF-DFA.

3.3. Reliable quantification of multi-fractal strength

When we use ΔA_q to quantify the multicractality, the calculation of ΔA_q is no matter with estimation of $H(2)$. Thereby, the error caused by DFA procedure to obtain $H(2)$ has no relationship with ΔA_q. Therefore, when we compare the effects between the two methods, we can use the theoretical value of $H(2)$ to convert A_q and ΔA_q of ESS-MF-DFA to $H(q)$ and ΔH_q, and compare with the results of MF-DFA.

Based on binomial multi-fractal model, the comparison between theoretical $H(q)$ and the estimated $H(q)$ from MF-DFA and ESS-MF-DFA can tell us which method works better in estimating the generalized Hurst exponents. More importantly, reasonable quantitative criterion based on ESS-MF-DFA is proposed to differentiate multi-fractal from mono-fractal behavior.

Table 2
Comparison between the theoretical value of Eq. (2) and $H(q)$ estimated from outputs of the binomial multi-fractal model with $a = 0.9$ by MF-DFA and ESS-MF-DFA.

q		−3	−2	−1	1	2	3
$H(q)$	Theoretical	2.9893	2.8308	2.4739	1.0000	0.6432	0.4847
	MF-DFA	2.9776	2.8096	2.4027	0.9946	0.6230	0.4586
	ESS-MF-DFA	2.9812	2.8127	2.4012	1.0040	0.6432	0.4813

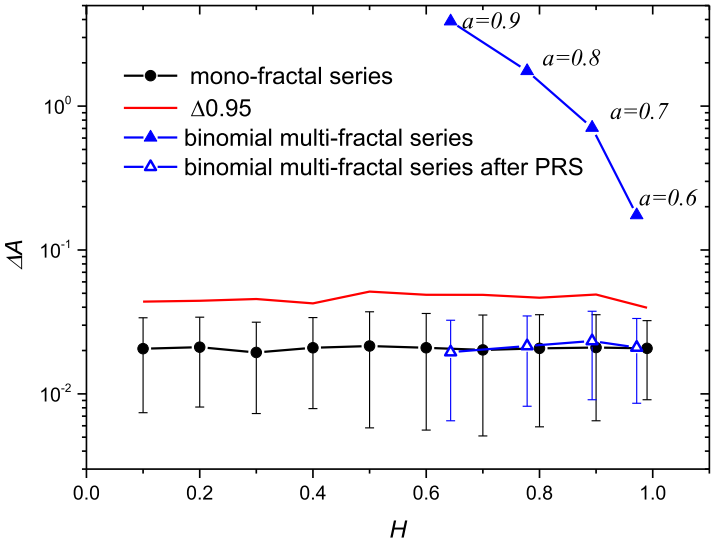

Fig. 6. Criterion to distinguish multi-fractal from mono-fractal behavior and its check by outputs of binomial multi-fractal model. The black circle means $\overline{\Delta A}$ over 100 repeated mono-fractal simulations from $H = 0.1$ to $H = 0.99$ with the error bar showing $\sigma_{\Delta A}$. The red line means the varying range of $\Delta A(q)$ when 95% of all the samples are included, which determines the criterion $\Delta_{0.95} \approx 0.05$. The blue solid triangle is ΔA estimated from binomial multi-fractal series with a from 0.6 to 0.9, with x-coordinate corresponding to theoretical $H(2)$. The blue open triangle is $\overline{\Delta A}$ estimated from over 100 repeated PRS binomial multi-fractal series. (For interpretation of the references to colour in this figure legend, the reader is referred to the web version of this article.)

From Eq. (2), $H(q)$ for each q can be derived theoretically for binomial series. In addition, the outputs from binomial multi-fractal model can be used to estimate $H(q)$ by MF-DFA, or $H(q) = A_q \times H(2)$ by ESS-MF-DFA, where $H(2)$ can be theoretically derived from Eq. (2). Detailed results for Eq. (2) with $a = 0.9$ are shown in Table 2, where it can be found that all the estimated exponents are underestimated compared with the theoretical ones. At the same time, it is obvious that the estimated exponents for each q from ESS-MF-DFA are much closer to the theoretical ones, but the estimated exponents for each q from MF-DFA depart much greatly from the theoretical ones, especially for certain q. Similar results can be found when $a = 0.6,\ 0.7,\ 0.8$ (results are not shown). From the above results, we know that $\Delta H_q = \Delta A_q * H(2)$ derived from ΔA_q by ESS-MF-DFA is much believable than ΔH_q calculated by MF-DFA.

For the measured time series, the true value of $H(2)$ is unknown, their multi-fractal behaviors can be quantified directly by ΔA_q from ESS-MF-DFA based on Eqs. (7) and (8). In order to determine whether a time series has a significantly multi-fractal behavior or not, a threshold of ΔA_q should be determined. According to Kantelhardt et al. [4], the mono-fractal model used in this paper can be taken as a typical model for mono-fractal series [4] to establish a threshold of ΔA_q. So 100 repeated simulations of mono-fractal model with each H changing from 0.1 to 0.99 to determine the criterion $\Delta_{0.95}$ as the threshold of ΔA_q, which is utilized to diagnose whether the multifractal behavior is significant or not at the confidence probability of 0.95. The red line in Fig. 6 represents the varying range of ΔA_q when 95% of all the samples are included. The result shows that the $\Delta_{0.95}$ and standard deviation of different Hurst exponents almost remain stable for all Hurst exponents from 0.1 to 0.99. Meanwhile, $\Delta_{0.95}$ also changes with sample size and reaches their saturated value when the sample size arrives at around 400, which is consistent with the results given in Ref. [10]. However, we find that the variation of $\Delta_{0.95}$ is less than 0.004 when the sample number varies from 100 to 1000, which is too small to cause significant difference. Thereby, our results from experiments of 100 repeated simulations are reasonable within the error range. In this paper, the criterion is taken as $\Delta_{0.95} \approx 0.05$, see Fig. 6. Therefore, if ΔA_q is larger than $\Delta_{0.95}$, the analyzed series has significant multi-fractal properties (within the confidence probability of 0.95).

The validity of the established criterion $\Delta_{0.95} \approx 0.05$ can be checked through the idealized binomial multi-fractal model. The results from ESS-MF-DFA for outputs of binomial multi-fractal model are in excellent agreement with the theoretical ones derived directly from Eq. (2). And all the computed multi-fractal measure ΔA_q is significantly distinguished from the mono-fractal behavior with all estimated ΔA_q larger than the established criterion $\Delta_{0.95} \approx 0.05$ (see Fig. 6). At the same time, if the outputs of binomial multi-fractal model is handled by phase randomize surrogate procedure (PRS) to remove

the multifractality of original outputs [23,24], and then the multifractality will be lost in the ESS-MF-DFA computations with all the averaged ΔA_q below $\Delta_{0.95}$ (Fig. 6). In binomial multi-fractal model, the larger the value of a, the smaller the theoretical $H(2)$, and the more marked the multifractal behavior. Even when $a = 0.6$, the multifractal behavior is really weak and difficult to distinguish from mono-fractal series [4], the estimated ΔA_q is still much larger than $\Delta_{0.95}$ in Fig. 6, which indicates that ESS-MF-DFA really works well in distinguish multi-fractal from mono-fractal behavior.

4. Conclusion and discussions

In this paper, we have developed a new ESS-MF-DFA method for identifying and quantifying multi-fractal behavior in time series. Since DFA or MF-DFA is based on a fundamental assumption that there exists power law relation between the fluctuation functions and the scale, the narrower scaling range will cause severe problem in estimating the (generalized) Hurst exponents. How to extend the scaling range is vital to reduce the uncertainties in estimating the (generalized) Hurst exponents, i.e., the wider scaling range, the smaller uncertainties. Incorporated ESS can help us to reach this goal by extending the scaling range and reducing the uncertainties in estimating the (generalized) Hurst exponents. For time series from complex systems or natural processes, sometimes the scaling range is too narrower to define, DFA or MF-DFA will fail to work, at this case ESS- MF-DFA may still work well (see Fig. 1 for details). In addition, we have proposed a criterion based on ESS-MF-DFA for discriminating multi-fractal from mono-fractal behavior and verified that it works well in distinguishing binomial multi-fractal series from their PRS series (see Fig. 6 for details).

Previous studies show that the violations of ESS should be due to the presence of strong shear in the flows [25], where non-stationary larger scale structures are playing an essential role in flows' statistics. While DFA and MF-DFA are methods developed for analysis of non-stationary time series [1–4,21,22], since ESS-MF-DFA is extended from DFA and MF-DFA, ESS-MF-DFA may still work well in this kind of cases.

Furthermore, the ESS-MF-DFA method can be used to not only boundary layer wind speed, but also stratospheric variability [26], output of nonlinear systems and other similar systems. The scaling ranges in these systems are too narrower to define or there is even no scaling range, which makes the fundamental assumption in DFA and MF-DFA is invalid. The applications of ESS-MF-DFA to these fields also deserve to be further explored in future.

Acknowledgments

The authors acknowledge the supports from National Natural Science Foundation of China (Nos. 41475048, 41675049).

References

[1] Peng CK, Havlin S, Stanley HE, Buldyrev SV, Sciortino F, Goldberger AL, Simons M. Long-range correlations in nucleotide sequences. Nature 1992;356:168–70.
[2] Peng CK, Buldyrev SV, Havlin S, Simons M, Stanley HE, Goldberger AL. Mosaic organization of DNA nucleotides. Physical Review E 1994;49(2):1685–9.
[3] Talkner P, Weber RO. Power spectrum and detrended fluctuation analysis: application to daily temperatures. Physical Review E 2000;62:150–60.
[4] Kantelhardt JW, Zschiegner SA, Koscielny-Bunde E, Havlin S, Bunde A, Stanley HE. Multifractal detrended fluctuation analysis of nonstationary time series. Physica A 2002;316:87.
[5] Telesca L, Lovallo M. Analysis of the time dynamics in wind records by means of multifractal detrended fluctuation analysis and the Fisher–Shannon information plane. J Stat Mech 2011;2011:P07001.
[6] Li J, Wei H, Fan L, Wei L. Multifractal detrended fluctuation analysis of frictional vibration signals in the running-in wear process. Tribol Lett 2017;65(2):1–9.
[7] Miriyala S, Koppireddi PR, Chanamallu SR. Robust detection of ionospheric scintillations using MF-DFA technique. Earth Planets Space 2015;67(1):1–5.
[8] Dong Q, Wang Y, Li P. Multifractal behavior of an air pollutant time series and the relevance to the predictability. Environ Pollut 2017;222:444–57.
[9] Gulich D, Zunino L. A criterion for the determination of optimal scaling ranges in DFA and MF-DFA. Physica A 2014;397:17–30.
[10] Yuan NM, Fu ZT, Mao JY. Different multi-fractal behaviors of diurnal temperature range over the north and the south of china. Theor Appl Climatol 2013;112:673–82.
[11] Shao Y, Gu G, Jiang Z, Zhou W, Sornette D. Comparing the performance of FA, DFA and DMA using different synthetic long-range correlated time series. Sci Rep 2012;2:835.
[12] Zeng M, Zhang X, Li J, Meng Q. the scaling properties of high-frequency wind speed records based on multiscale multifractal analysis. Acta Phys Pol B 2016;47(9):2205–24.
[13] Benzi R, Ciliberto S, Tripiccione R, Baudet C, Massaioli F, Succi S. Extended self-similarity in turbulent flows. Physical Review E 1993;48(1):R29–32.
[14] Feder J. Fractals. New York: Plenum Press; 1988.
[15] Chen J, Hu F. Coherent structures detected in atmospheric boundary-layer turbulence using wavelet transforms at Huaihe river basin, China. Boundary Layer Meteorol 2003;107:429–44.
[16] Li QL, Fu ZT. Permutation entropy and statistical complexity quantifier of nonstationarity effect in the vertical velocity records. Physical Review E 2014;89:012905.
[17] Chen H, Chen J, Hu F, Zeng Q. The coherent structure of water vapour transfer in the unstable atmospheric surface layer. Boundary Layer Meteorol 2004;111:543–52.
[18] Li X, Hu F, Liu G. Characteristics of chaotic attractors in atmospheric boundary-layer turbulence. Boundary Layer Meteorol 2001;99:335–45.
[19] Fu ZT, Li Q, Yuan NM, Yao ZH. Multi-scale entropy analysis of vertical wind variation series in atmospheric boundary-layer. Commun Nonlinear Sci Numer Simul 2014;19:83–91.
[20] Wang JY, Fu ZT, Zhang L, Liu SD. Information entropy analysis on turbulent temperature series in the atmospheric boundary layer. Plateau Meteorol 2005;24(1):38–42.
[21] Hu K, Ivanov PC, Chen Z, Carpena P, Stanley HE. Effect of trends on detrended fluctuation analysis. Phys Rev E 2001;64:011114–19.
[22] Chen Z, Ivanov PC, Hu K, Stanley HE. Effect of nonstationarities on detrended fluctuation analysis. Phys Rev E 2002;65:041115–17.

[23] Ashkenazy Y, Ivanov PC, Havlin S, Peng C, Goldberger AL, Stanley HE. Magnitude and sign correlations in heartbeat fluctuations. Phys Rev Lett 2001;86:1900–3.
[24] Ashkenazy Y, Havlin S, Ivanov PC, Peng C, Schulte-Frohlinde V, Stanley HE. Magnitude and sign scaling in power-law correlated time series. Physica A 2003;323:19–41.
[25] Benzi R, Biferale L, Ciliberto S, Struglia MV, Tripiccione R. Generalized scaling in fully developed turbulence. Physica D 1996;96:162–81.
[26] Fu ZT, Shi L, Xie FH, Piao L. Nonlinear features of northern annular mode variability. Physica A 2016;449:390–4.